

LLaDA-MedV: Exploring Large Language Diffusion Models for Biomedical Image Understanding

Xuanzhao Dong^{1*} Wenhui Zhu^{1*} Xiwen Chen^{2*} Zhipeng Wang^{3*} Peijie Qiu⁴ Shao Tang³
Xin Li¹ Yalin Wang¹

¹ Arizona State University, AZ, USA

² Clemson University, SC, USA

³ LinkedIn Corporation, CA, USA

⁴ Washington University in St. Louis, MO, USA

Abstract

Autoregressive models (ARMs) have long dominated the landscape of biomedical vision-language models (VLMs). Recently, masked diffusion models such as LLaDA have emerged as promising alternatives, yet their application in the biomedical domain remains largely underexplored. To bridge this gap, we introduce **LLaDA-MedV**, the first large language diffusion model tailored for biomedical image understanding through vision instruction tuning. LLaDA-MedV achieves relative performance gains of 7.855% over LLaVA-Med and 1.867% over LLaDA-V in the open-ended biomedical visual conversation task, and sets new state-of-the-art accuracy on the closed-form subset of three VQA benchmarks: 84.93% on VQA-RAD, 92.31% on SLAKE, and 95.15% on PathVQA. Furthermore, a detailed comparison with LLaVA-Med suggests that LLaDA-MedV is capable of generating reasonably longer responses by explicitly controlling response length, which can lead to more informative outputs. We also conduct an in-depth analysis of both the training and inference stages, highlighting the critical roles of initialization weight selection, fine-tuning strategies, and the interplay between sampling steps and response repetition. The code and model weight is released at <https://github.com/LLM-VLM-GSL/LLaDA-MedV>.

1. Introduction

Building on the success of general domain vision-language models (VLMs), researchers have increasingly shifted their focus to the biomedical domain, leading to the development of biomedical VLMs that have demonstrated notable

progress across a variety of medical tasks [3, 22, 53]. Notably, autoregressive models (ARMs), known for their effectiveness in modeling multimodal distributions, currently dominate the biomedical VLM landscape, particularly in scenarios that require text generation grounded in visual understanding. This prevalence naturally motivates the exploration of alternative generative paradigms. Recently,

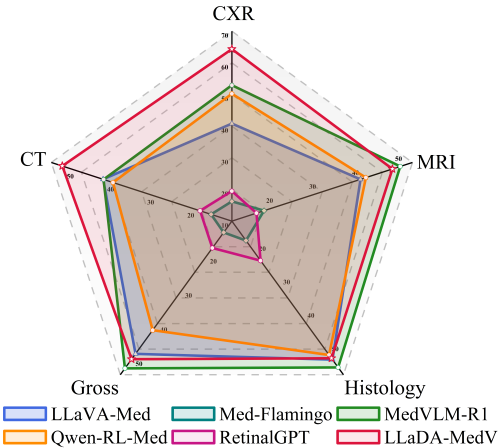


Figure 1. Illustration of biomedical VLMs evaluated in the open-ended biomedical conversation benchmark. Among the 6 Medical VLMs, LLaDA-MedV achieves the highest overall score and demonstrates the best performance on Chest X-ray (CXR) and CT modalities.

masked diffusion models (MDMs) [28, 42, 43] have shown significant promise in language generation. In particular, LLaDA [33] have emerged as a compelling alternative. Unlike continuous-state diffusion models [15, 44, 45], which operate over continuous data (e.g., image pixels), it operate directly on discrete tokens. In the forward process, it replaces input tokens with a special `<mask>` tokens,

*These authors contributed equally to this paper.

which acts as an absorbing state. In the reverse generation process, the model predicts the masked content simultaneously, progressively refining the sequence across multiple steps. Notably, with large-scale training, LLaDA-based models [33, 56] have already demonstrated strong scalability and competitive performance in the general domain.

Although language diffusion models have shown strong performance in general domains, applying them to biomedical image understanding remains nontrivial. The core difficulty lies in the substantial domain gap between general and biomedical data. To move forward, we must first address several key questions critical to building effective biomedical diffusion VLMs:

- *How can the success of language diffusion models in the general domain be effectively adapted to biomedical image understanding?*
- *Why are language diffusion models promising for biomedical vision-language modeling?*
- *What design principles are essential for developing effective biomedical diffusion VLMs?*

To address these questions, we first introduce **LLaDA-MedV**, a large language diffusion model specifically developed for biomedical visual understanding. LLaDA-MedV demonstrates strong visual understanding ability. As shown in Fig. 1, the model outperforms several autoregressive baselines on open-ended biomedical visual conversation tasks, following semantic alignment and supervised fine-tuning. Second, we conduct a comparative analysis between LLaDA-MedV and LLaVA-Med [19]. Our results show that LLaDA-MedV produces significantly longer and more detailed responses, while also enabling explicit control over output length, which is an important feature for tasks that demand comprehensive answers. Finally, we further perform an in-depth analysis of the training and inference pipelines to identify the key factors underlying the model performance. On the training setting, we find that proper initialization and domain-specific fine-tuning are critical. During inference, we analyze the role of sampling steps and observe that they substantially impact output diversity, especially in longer sequence generation.

In summary, our key contributions are as follows:

- We present **LLaDA-MedV**, the first diffusion-based vision-language model designed for biomedical image understanding via visual instruction tuning.
- We provide a comprehensive empirical study comparing LLaDA-MedV with autoregressive counterparts across open-ended biomedical conversations and VQA tasks, showing consistent advantages in response quality and controllability.
- We conduct in-depth analysis of training and inference behavior of LLaDA-MedV, identifying several design factors that affect generation performance (e.g., sampling and initialization). These findings offer valuable insights

for future research on diffusion-based language models, particularly in biomedical field.

2. Related Work

2.1. Large Language Diffusion Models

Recent advancements in diffusion models for vision tasks have spurred growing interest in their application to natural language processing. However, adapting diffusion models to language presents unique challenges due to the discrete nature of language tokens, which contrasts with the continuous pixel representations in vision tasks. To address this, several studies have proposed learning continuous representations of textual data [6, 9, 30, 41, 46, 55]. Moreover, Diffusion-LM [21] introduces a method to denoise sequences of Gaussian vectors into word embeddings using learned bidirectional mappings. In parallel, other works focus on discrete diffusion frameworks, particularly masked diffusion models (MDMs) [10, 36]. Notably, LLaDA [33] marks a significant milestone by scaling MDMs to 8B parameters and achieving competitive results compared to ARM baselines such as LLaMA3 [11].

Despite these promising developments, most diffusion-based language models are restricted to text-only applications. Their potential in multimodal contexts, especially in the biomedical domain, remains largely unexplored. This gap forms the basis for our work, which aims to extend the benefits of language diffusion models to the biomedical domain.

2.2. BioMedical VLMs

Biomedical VLMs typically leverage existing general-domain architectures either by training from scratch or through domain-specific fine-tuning [17, 32, 38]. For instance, BiomedGPT [29, 57] adopts a GPT-style autoregressive architecture and is trained from scratch on large-scale biomedical multimodal datasets, achieving strong performance across several biomedical benchmarks. In addition to large-scale training strategies that demand substantial computational resources, prompt learning and prompt engineering have emerged as efficient alternatives [7, 12, 52]. For example, ChatCAD [51] integrates large language models into computer-aided diagnosis systems, generating clinically grounded outputs to support decision-making.

While these methods have advanced the field significantly, most biomedical VLMs to date rely on autoregressive modeling. The potential of discrete diffusion models, particularly MDMs, remains largely untapped in biomedical applications. To address this gap, we propose LLaDA-MedV, the first biomedical VLM based on masked diffusion modeling. Furthermore, our work opens a new direction for scalable, effective biomedical image-language understanding using diffusion-based LLM model.

3. Preliminary

3.1. Masked Diffusion Models

Masked diffusion models (MDMs) operate over discrete tokens (e.g., text) using a structured forward-reverse process defined over a finite support. In LLaDA, a special mask token $\langle\text{mask}\rangle := \mathbf{M}$ is introduced, which serves as an absorbing state in the transition matrix. Intuitively, as the time step t increases, each token either remains unchanged or transitions to \mathbf{M} with probability t [1, 33]. This forward process can be formally described as:

$$q_{t|0}(x_t | x_0) = \prod_{i=1}^L q_{t|0}(x_t^i | x_0^i) \quad (1)$$

$$\text{where } q_{t|0}(x_t^i | x_0^i) = \begin{cases} 1 - t, & x_t^i = x_0^i \\ t, & x_t^i = \mathbf{M} \end{cases}$$

Thus, as t increases, a greater proportion of tokens are replaced by the mask token \mathbf{M} . Analogous to denoising score matching in continuous diffusion models [50], the reverse process in LLaDA seeks to reconstruct the original sequence from a fully masked sequence. Specifically, for a reverse step where $0 \leq s < t \leq 1$, the conditional transition is defined as:

$$q_{s|t}(x_s | x_t) = \prod_{i=1}^L q_{s|t}(x_s^i | x_t) \quad \text{where} \quad (2)$$

$$q_{s|t}(x_s^i | x_t) = \begin{cases} 1, & x_t^i \neq \mathbf{M}, x_s^i = x_t^i \\ \frac{s}{t}, & x_t^i = \mathbf{M}, x_s^i = \mathbf{M} \\ (1 - \frac{s}{t})q_{0|t}(x_s^i | x_t) & x_t^i = \mathbf{M}, x_s^i \neq \mathbf{M} \\ 0 & \text{otherwise} \end{cases}$$

This formulation intuitively captures the behavior of the reverse process: it retains the unmasked tokens, maintains a portion s/t of the masked tokens as masks, and samples the remaining $(1 - s/t)$ proportion from $q_{0|t}(\cdot)$. [36] propose an efficient approach to compute $q_{0|t}(\cdot)$ based on clean data prediction, such that $q_{0|t}(x_s^i | x_t) = p_d(x_0^i | x_t)$ for all positions where $x_t^i = \mathbf{M}$. To model the unknown data distribution $p_d(\cdot)$, a mask predictor $p_\theta(\cdot | x_t)$ is introduced. The learning objective follows the formulations proposed in [28, 33]:

$$\mathcal{L}_\theta^0 := -\mathbb{E}_{t,x_0,x_t} \left[\frac{1}{t} \sum_{i=1}^L \mathbf{1}[x_t^i = \mathbf{M}] \log p_\theta(x_0^i | x_t) \right] \quad (3)$$

Here, $\mathbf{1}[\cdot]$ is the indicator function and $t \sim \mathcal{U}[0, 1]$. At inference time, generation proceeds as motivated by Eq. 2.

Beginning with a fully masked sequence (i.e., $t = 1$), the model uses learned $p_\theta(x_0 | x_t)$ to iteratively reconstruct the clean sequence. A remasking step is applied at each stage to ensure alignment with the theoretical reverse dynamics (i.e., retain s/t portion masked components). This denoising process continues until the final step, resulting in a fully reconstructed output.

3.2. Visual Instruction Tuning

Rather than training VLMs from scratch, visual instruction tuning [24] (i.e., LLaVA) offers a more efficient paradigm for equipping a pretrained language backbone with visual understanding. This approach adopts a modular architecture comprising three key components: a language backbone $f_\phi(\cdot)$ (e.g., LLaMA [47]), a vision encoder $g(\cdot)$ (e.g., CLIP [39]), and a projection module $h(\cdot)$ (typically a lightweight MLP). Given a visual input X_v , the vision encoder first extracts high-level image features $g(X_v)$, which are then projected into the language embedding space via $h(\cdot)$ to produce $H_v = h(g(X_v))$. These vision embeddings are inserted into the language model’s input sequence, often prepended to the text prompt, and jointly processed by f_ϕ . This setup allows the language model to generate coherent, visually grounded responses conditioned on both image and text inputs, thereby achieving multimodal capabilities with minimal architectural modifications. To support effective training, the input data are typically formatted as single/multi-turn dialogues that simulate interactions between a human user and an AI assistant [19, 24, 25].

4. Methods

4.1. Training Architecture

Learning objective. For clarity, we describe the setup using a single image and a single-turn dialogue. Given training instance denoted by a tuple (X_v, u_0, r_0) , where X_v represent the image, $u_0 := [u_0^i]_{i=1}^{L_{u_0}}$ denote the user prompt (e.g., a biomedical query) of length L_{u_0} and $r_0 := [r_0^j]_{j=1}^{L_{r_0}}$ represents the ground-truth assistant response (e.g., generated by GPT) of length L_{r_0} . The training objective extends the original masked prediction formulation (i.e., Eq. 3) by conditioning on the user prompt and is defined as:

$$\mathcal{L}_\theta^1 := -\mathbb{E} \left[\frac{1}{t} \sum_{j=1}^{L_{r_0}} \mathbf{1}[r_t^j = \mathbf{M}] \log p_\theta(r_0^j | X_v, u_0, r_t) \right] \quad (4)$$

Here r_t denotes the masked response obtained from the clean response r_0 through forward masking, and we abuse notation by letting X_v also represent the corresponding visual embeddings for brevity. Intuitively, this objective trains the mask predictor p_θ to recover the masked portions of the assistant’s response based on both the user prompt and vi-

sual features. Following prior works [33, 56], we model p_θ by a Transformer architecture with bidirectional attention.

Multi-stage Training Pipeline. Training LLaDA-MedV consists of three stages. The first two stages aim to establish semantic alignment between biomedical language and visual content, and to equip the model with instruction-following capabilities for biomedical visual understanding. To further improve service quality in data-specific scenario, we perform an additional SFT stage using three biomedical VQA training datasets. Details of each stage are provided below:

- **Stage 1: Biomedical Semantic Alignment.** In this stage, we freeze both the vision tower and the language backbone, and fine-tune only the lightweight MLP projector. This step ensures that the extracted visual features are effectively projected into the language embedding space and semantically aligned with biomedical concepts.
- **Stage 2: End-to-End Vision Instruction Tuning.** After stage 1, we fine-tune the language backbone and the projector module to enable LLaDA-MedV the medical visual understanding and coherent response generation abilities. Unlike [56], we keep the vision tower frozen. Each training instance consists of a single image and its associated multi-turn dialogues.
- **Stage 3: Dataset Specific Fine-tuning.** To further improve model performance in scenario that require higher accuracy, we further fine-tune the model on three benchmarks [14, 18, 23]. Each training example is formatted as a single-turn dialogue between a human user and the assistant, following the same training setup as in Stage 2. This step enables LLaDA-MedV to provide free-form answers for both closed-form and open-ended biomedical questions. The vision tower remains frozen during this stage as well.

It is important to note that we do not adopt the initialization strategy used in [19]. In our experiments, initializing from weights [56] degraded the model’s ability to interpret medical images and led to repetitive output generation. ***For implementation details, please refer to the Appendix A.***

4.2. Inference Architecture

Generating responses simulates the reverse dynamics (as defined in Eq. 2). Beginning with a fully masked response, the learned mask predictor p_θ progressively reconstructs the response content, accompanied by appropriate remasking to align with the reverse diffusion process. Following prior works [33, 56], we adopt low-confidence remasking strategy [5], where only tokens with low confidence (i.e., lower p_θ values) are remasked. In addition, we also explore a semi-autoregressive generation strategy [33]. Specifically, a response of length L is divided into L/B blocks, where B denotes the block length. The generation process is applied sequentially from left to right across these blocks, with each

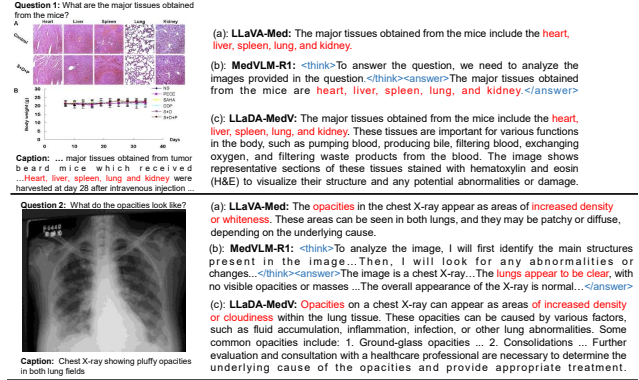


Figure 2. Illustration of open-end conversation evaluation. All questions, images and corresponding captions are sourced from [19]. We present representative responses from (a) LLaVA-Med, (b) MedVLM-R1, and (c) LLaDA-MedV. Key informative segments are highlighted in red for emphasis.

block undergoing $Z \cdot B/L$ sampling steps. ***We provide the detailed inference algorithm in Appendix A.***

5. Experiments

5.1. Experimental Setup and Configuration

Dataset and Configuration. Training LLaDA-MedV involves three stages. In Stage 1, we use 600k alignment text-image pairs. In Stage 2, we employ a 60k multi-turn inline-mention dialogue dataset, selected for its consistently strong performance. In Stage 3, we further fine-tune the model using the training sets from VQA-RAD [18], SLAKE [23], and PathVQA [14], following the official data splits provided in [19]. For the model architecture, we use LLaDA-8B-Instruct [33] as the language backbone. The vision tower is based on SigLIP2 [48], and visual-language projector is implemented as a lightweight two-layer MLP with GELU activation. All training is performed on four NVIDIA A100 80GB GPUs.

For evaluation, we set the hyperparameters to $L = 256$, $B = 64$, and $Z = 256$ for open-ended biomedical conversation evaluation. To ensure fair comparison, we also set the maximum token length to 256 for all baseline models. For the three downstream biomedical VQA tasks, we use $L = B = Z = 64$ to ensure computational efficiency, and directly report the official scores of the baseline models as reported in [19]. Unless otherwise specified, these parameter settings are used consistently across all experiments. ***Additional details are provided in the Appendix A.***

5.2. Open-end Biomedical Conversation

We adopt the Biomedical Visual Chatbot benchmark [19] to evaluate the performance of LLaDA-MedV in a realistic open-ended conversation setting. Specifically, we use

	Question Types		Domains					Overall (193)
	Conversation (143)	Description (50)	CXR (37)	MRI (38)	Histology (44)	Gross (34)	CT (40)	
LLaMA [31]	27.850	27.750	33.505	23.841	24.684	31.764	26.458	27.824
LLaVA [24]	43.509	29.671	45.935	41.761	42.726	33.905	33.4	34.653
LLaVA-Med [19]	51.750	24.730	40.819	39.928	51.452	48.880	42.083	44.750
Med-Flamingo [32]	16.339	13.702	16.238	17.502	15.823	13.311	15.174	15.656
MedVLM-R1 [38]	52.774	42.663	52.944	49.159	53.801	53.122	41.984	50.154
Qwen-RL-Med [59]	46.408	40.016	50.225	41.181	50.081	41.929	39.618	44.752
Qwen-VL [2]	51.546	40.143	58.929	43.186	51.344	47.106	42.401	48.592
RetinalGPT [60]	20.535	13.349	19.477	15.722	21.839	17.875	17.932	18.673
LLaDA-V [56]	53.574	42.627	57.545	38.445	64.191	49.055	42.753	50.738
Ours	54.141	48.214	64.352	47.348	51.073	50.432	50.268	52.605

Table 1. Illustration of results on the open-ended biomedical conversation benchmark across several VLM baselines. CXR refers to Chest X-ray. Scores reflect relative performance against GPT-4 responses, as judged by GPT-4.1. For models with intermediate reasoning steps, we include all content for fair comparison.

GPT-4.1 mini [34]^{*} as the evaluator. It assesses the model-generated responses by comparing them to reference answers produced by GPT-4 [35], assigning a relative score to each response, where higher scores indicate better performance.

LLaDA-MedV demonstrates superior ability in following visual instructions and generating informative responses. As shown in Tab. 1, it outperforms both LLaVA-Med and MedVLM-R1 across nearly all subjects, achieving overall performance gains of 7.855% and 2.45%, respectively. Furthermore, we observe that LLaDA-MedV tends to produce longer responses compared to ARM baselines. For instance, as illustrated in Question 2 of Fig. 2, instead of merely describing the appearance of opacities, LLaDA-MedV also provides relevant contextual information such as potential causes, common categories, and a cautious recommendation for further consultation. **We provide more case studies in Appendix B.**

Two additional points warrant clarification. First, unlike other ARM baselines (e.g., LLaVA-Med over LLaMA), our language backbone (i.e., LLaDA) is trained solely via pretraining and SFT, without any post-training such as reinforcement learning (RL) [13] or human preference tuning [37]. Second, although AI assistants such as GPT are not perfect evaluators, their use has become standard practice in the community [16, 19, 26, 54]. Therefore, we believe our comparative evaluation remains fair and sufficiently rigorous to demonstrate the advantages of our approach in biomedical field.

^{*}We use GPT-4.1 mini for evaluation because the original GPT-4 (i.e., GPT-4-0314) model used in [19] is no longer accessible. As a result, we re-evaluate all baseline models rather than relying on their originally reported scores.

5.3. Downstream Visual Question Answering

We evaluate model performance on three biomedical visual question answering (VQA) benchmarks, which are designed to assess the model’s accuracy in clinically relevant scenarios. We follow the evaluation strategy proposed in [19]. For closed-form questions (e.g., Yes/No), we report accuracy. For open-form questions, we report recall, measuring the proportion of ground-truth tokens present in the generated sequence.

LLaDA-MedV demonstrates competitive performance compared to ARM baselines. As shown in Tab. 2, our model achieves the highest accuracy on closed-form questions across all three benchmarks, with scores of 84.93% on VQA-RAD, 92.31% on SLAKE, and 95.15% on PathVQA. However, performance on open-form questions remains less competitive. We observe that answering open-form questions in the VQA setting is inherently more challenging for our model, as the underlying language backbone (i.e., LLaDA) lacks sufficient post-training. Consequently, LLaDA-MedV struggles to model open-form questions as a classification task over a predefined answer set derived from the training split, which is the strategy commonly adopted in prior works [19]. Despite this limitation, the results underscore LLaDA-MedV’s potential in dataset-specific biomedical applications, motivating future efforts to improve its instruction-following and answer-formatting capabilities through post-training (e.g., reinforcement learning from human feedback [37]).

Model	VQA-RAD		SLAKE		PathVQA	
	Open	Closed	Open	Closed	Open	Closed
LLaVA	50.00	65.07	78.18	63.22	7.74	63.20
LLaVA-Med (From LLaVA)	61.52	84.19	83.08	85.34	37.95	91.21
VL Encoder-Decoder [4]	71.49	82.47	-	-	71.49	85.61
Q2ATransformer [27]	79.19	82.47	-	-	54.85	88.85
Prefix T. Medical LM [49]	-	-	84.30	82.01	40.00	87.00
PubMedCLIP [8]	60.10	80.00	78.40	82.50	-	-
BiomedCLIP [58]	67.60	79.80	82.05	89.70	-	-
M2I2 [20]	66.50	83.50	74.70	91.10	36.30	88.00
Ours	45.60	84.93	68.85	92.31	31.96	95.15

Table 2. Illustration of results on downstream VQA tasks. For all baselines, we report results directly when available. Following [19], we use token-level recall for open-form questions and answer accuracy for closed-form ones. Prior models often treat open-form questions as classification over a fixed answer set, raising concerns about generalizability. In contrast, due to limited post-training, LLaDA-MedV may struggle to perform reliable classification over predefined candidate sets, instead producing more open-ended responses that are harder to constrain within rigid answer formats.

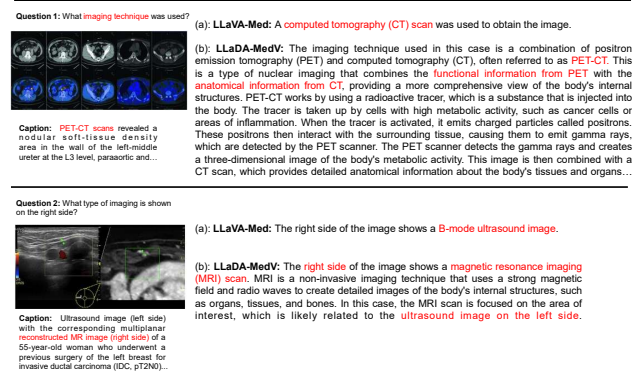


Figure 3. Illustration of LLaVA-Med and LLaDA-MedV responses to biomedical queries 1 and 2. The images, queries, and corresponding captions are adapted from [19]. For fair comparison, the generation lengths are aligned by setting the maximum token limit to the same value (e.g., generation length $L = 256$).

6. Analysis

6.1. Why Language Diffusion Models?

ARMs typically control response length through heuristics such as adjusting the maximum token limit or modifying the system prompt. However, this method often proves unreliable in biomedical contexts. For example, models like LLaVA-Med frequently terminate early when an end-of-sequence token is predicted prematurely, resulting in responses that are shorter than expected and lacking in detail. As shown in Tab. 3, LLaDA-MedV generates an aver-

OE Conversation (193)	T/Q	W/Q	T/W	Z	Overall Score
LLaVA-Med	1.317	36.332	0.036	-	44.750
LLaVA-Med ²⁰⁰	1.392	40.922	0.034	-	44.582
LLaDA-MedV ₂₅₆	38.382	166.585	0.230	256	52.605
LLaDA-MedV ₁₂₈	30.874	170.399	0.181	128	44.276
LLaDA-MedV ₆₄	21.234	172.839	0.123	64	28.523
LLaDA-MedV ₃₂	13.945	182.596	0.076	32	18.581
LLaDA-MedV ₁₆	8.595	192.09	0.045	16	13.525

Table 3. Illustration of open-ended (OE) conversation evaluation on 193 questions. **T/Q** is the average response time per question (in seconds), **W/Q** is the average word count, and **T/W** is the average time per word. LLaVA-Med²⁰⁰ uses a modified prompt encouraging responses of at least 200 words. For LLaDA-MedV, we fix the generation length $L = 256$ and block size $B = 64$, and vary the sampling steps Z from 16 to 256 during inference.

age of 166 words per response, whereas LLaVA-Med generates only around 36. To examine whether prompt engineering could extend response length in LLaVA-Med, we introduced a system prompt explicitly requesting at least 200 words per answer. Despite this, the model's output increased only marginally, reaching approximately 40 words per response. These findings suggest that ARMs offer limited control over output length in practice.

In contrast, LLaDA-MedV follows a different generation process. It begins with a fully masked sequence of fixed length and gradually fills in the tokens through iterative denoising. This design enables the model to explicitly control the length of the generated response, resulting in outputs that are both longer and more complete. As illustrated in

Fig. 3, the model not only identifies the imaging modality correctly (e.g., PET/CT) but also explains how PET is combined with CT, providing helpful contextual insights absent from ARM-based outputs. This increase in content is reflected in automatic evaluation scores. As reported in Tab. 1, LLaDA-MedV achieves a 7.855% improvement in response quality compared to LLaVA-Med. LLaDA-MedV requires more computation. As shown in Tab. 3, it raises inference time per word from 0.036 seconds to 0.230 seconds. However this trade-off is reasonable given the improved output quality. Moreover, the current implementation of LLaDA-MedV is not yet optimized, and we anticipate significant gains in efficiency with further engineering. Overall, these results demonstrate that masked language diffusion offers more reliable control over response length and content, which is particularly valuable for biomedical applications that demand detailed and context-rich answers.

Model	OE Conversation		VQA-RAD		SLAKE	
	Overall Score		Open	Ended	Open	Ended
LLaVA-Med*	44.750		28.23	61.40	39.17	52.16
LLaDA-MedV*	52.605		39.34	75	45.96	67.31
LLaDA-MedV ^{V1}	31.123		-	-	-	-
LLaDA-MedV ^{V2}	31.056		-	-	-	-

Table 4. Illustration of performance in analyzing the training pipeline. LLaVA-Med* and LLaDA-MedV* are trained with only alignment and SFT. LLaDA-MedV^{V1} uses LLaDA-V initialization and is trained with SFT only. LLaDA-MedV^{V2} also starts from LLaDA-V but includes both alignment and SFT. All LLaDA-based models use identical training and inference settings as main experiments. Due to the large performance gap, no further fine-tuning were performed on LLaDA-MedV^{V1} and LLaDA-MedV^{V2}.

6.2. Training-Time Considerations

Task-specific fine-tuning plays an important role in optimizing performance for specialized biomedical benchmarks. As shown in Tab. 4, although LLaDA-MedV outperforms LLaVA-Med in zero-shot settings on the VQA-RAD and SLAKE benchmarks, a clear performance gap remains when compared to fine-tuned models (Tab. 2). These findings suggest that fine-tuning can provide substantial benefits in improving performance and enhancing assistant capabilities in biomedical scenarios.

The choice of initialization weights also appears to influence performance. Our experiments indicate that initializing LLaDA-MedV with LLaDA-V, which is trained on general image and video understanding tasks, results in suboptimal performance, even after supervised fine-tuning (Tab. 4). Both LLaDA-MedV^{V1} (without alignment) and LLaDA-MedV^{V2} (with alignment) perform worse than LLaDA-MedV*, suggesting that general-domain priors may not fully align with biomedical semantics. Addition-

ally, as illustrated in question 4 and 5 of Fig. 4, these variants are more prone to generating repetitive responses under identical settings. Together, these findings highlight the importance of selecting domain-appropriate initialization strategies and incorporating fine-tuning to effectively adapt diffusion-based models to biomedical applications.

Group	Hyperparameters				Open-end Conversation Overall Score
	L	B	Z	$Z \cdot B/L$	
(A)	32	32	32	32	37.057
	64	32	64	32	39.135
	128	32	128	32	33.222
	256	32	256	32	51.215
(B)	256	256	32	32	20.165
	256	256	64	64	31.774
	256	256	128	128	44.020
	256	256	256	256	51.470
(C)	256	32	256	32	51.215
	256	64	256	64	52.605
	256	128	256	128	51.641
	256	256	256	256	51.470

Table 5. Performance under different hyperparameter configurations. Gray cells denote the setting outlined in Tab. 1. L represents the generation length, B denotes the block length, and Z indicates the total sampling steps. The term $Z \cdot B/L$ corresponds to the sampling steps per block.

6.3. Inference-Time Key Factors

We next examine how inference-time factors affect the quality and efficiency of generated responses. Specifically, we study the impact of generation length, the number of sampling steps, and block length within the semi-autoregressive generation process, where applicable. To investigate the effect of response length in real-world open-ended scenarios, we progressively increased the generation length L while keeping the number of sampling steps per block fixed. As shown in Tab. 5(A), we found out that increasing L from 32 to 256 results in fluctuating performance, rather than the insensitivity reported in previous work (e.g., [33]). This discrepancy may initially criticize our experiments (i.e., Tab. 1), as longer responses typically provide richer context to GPT-based evaluators, which could improve perceived answer quality. However, we emphasize that our evaluation is conducted under a controlled setting in which all models are encouraged to produce responses of fixed length (i.e., $L = 256$). For ARMs such as LLaVA-Med, this is enforced by setting the maximum token length to 256. In contrast, LLaDA-MedV’s masked prediction mechanism inherently promotes the generation of more complete and informative responses under the same length constraint. Furthermore, differences in benchmark design and evaluation protocols may also contribute to the observed variation in performance trends.

Second, we observe that the number of sampling steps

Figure 4. Illustration of token repetition during generation (i.e., mark by red) across different settings. Question 4 and 5 represent the answer from LLaDA-MedV^{V1} and LLaDA-MedV^{V2}, respectively. We omit the corresponding images for clarity.

Z introduces a trade-off between generation quality and computational efficiency. Generating a full response requires Z sampling steps. Naturally, reducing Z lowers the time cost associated with reconstructing the original content r_0 . As shown in Tab. 3, when Z gradually decreases, the average generation time per word decreases 5 times with the compensation of clear performance drop (also noted in Tab. 5(B)). This outcome is intuitive, as fewer steps introduce more noise into the reverse generative process described in Eq. 2.

Finally, we find that the block length B requires careful tuning in the semi-autoregressive generation setting. When $B < L$, the model applies semi-autoregressive generation. However, as shown in Tab. 5(C), increasing B , and thus increasing the number of sampling steps per block (i.e., $Z \cdot B/L$), does not consistently improve performance. This observation underscores the need for further investigation into optimal block configurations and their interaction with sampling dynamics. *Additional visualizations are provided in Appendix B.*

6.4. Limitation and Future Works

In addition to the findings discussed above, we observe a key limitation that merits further investigation: token repetition during generation. As shown in Fig. 4, the model exhibits a tendency to repeat tokens excessively under certain conditions. For instance, in Questions 2 and 3, the word “the” appears repeatedly until the target output length is reached. This issue becomes more pronounced when the desired response length is large, but the number of sampling steps is relatively small. One intuitive explanation is that when the number of sampling steps is insufficient, the

model has fewer opportunities to remask and refine low-confidence tokens. Consequently, early generation errors or repetitive patterns are likely to persist throughout the generation process. Furthermore, because the response length L imposes an upper bound on the number of total sampling steps (i.e., $Z \leq L$), this creates an inherent trade-off between generation quality and computational efficiency in long-form response settings. These observations suggest a need for better strategies to balance L and Z during inference. Future work may explore adaptive step allocation or more effective remasking schedules to reduce repetition while preserving efficiency, especially in applications that require lengthy and detailed outputs.

7. Conclusion

In this work, we introduce LLaDA-MedV, the first large language diffusion model designed for biomedical image understanding. Leveraging visual instruction tuning, LLaDA-MedV demonstrates competitive performance relative to ARMs across both open-ended biomedical conversation tasks and downstream biomedical VQA, underscoring its potential as a reliable biomedical AI assistant. Our analysis further emphasizes the critical roles of initialization weight selection, data-specific fine-tuning, and sampling step configuration in optimizing performance. Enhancing inference efficiency and mitigating token repetition represent important avenues for future research.

References

- [1] Jacob Austin, Daniel D Johnson, Jonathan Ho, Daniel Tarlow, and Rianne Van Den Berg. Structured denoising diffusion models in discrete state-spaces. *Advances in neural information processing systems*, 34: 17981–17993, 2021. 3
 - [2] Jinze Bai, Shuai Bai, Shusheng Yang, Shijie Wang, Sinan Tan, Peng Wang, Junyang Lin, Chang Zhou, and Jingren Zhou. Qwen-vl: A versatile vision-language model for understanding, localization, text reading, and beyond. *arXiv preprint arXiv:2308.12966*, 2023. 5, 13
 - [3] Shruthi Bannur, Stephanie Hyland, Qianchu Liu, Fernando Perez-Garcia, Maximilian Ilse, Daniel C Castro, Benedikt Boecking, Harshita Sharma, Kenza Bouzid, Anja Thieme, et al. Learning to exploit temporal structure for biomedical vision-language processing. In *Proceedings of the IEEE/CVF Conference on Computer Vision and Pattern Recognition*, pages 15016–15027, 2023. 1
 - [4] Yakoub Bazi, Mohamad Mahmoud Al Rahhal, Laila Bashmal, and Mansour Zuaire. Vision-language model for visual question answering in medical imagery. *Bioengineering*, 10(3):380, 2023. 6

- [5] Huiwen Chang, Han Zhang, Lu Jiang, Ce Liu, and William T Freeman. Maskgit: Masked generative image transformer. In *Proceedings of the IEEE/CVF conference on computer vision and pattern recognition*, pages 11315–11325, 2022. [4](#), [12](#)
- [6] Ting Chen, Ruixiang Zhang, and Geoffrey Hinton. Analog bits: Generating discrete data using diffusion models with self-conditioning. *arXiv preprint arXiv:2208.04202*, 2022. [2](#)
- [7] Stefan Denner, Markus Bujotzek, Dimitrios Boulias, David Zimmerer, Raphael Stock, and Klaus Maier-Hein. Visual prompt engineering for vision language models in radiology. *arXiv preprint arXiv:2408.15802*, 2024. [2](#)
- [8] Sedigheh Eslami, Christoph Meinel, and Gerard De Melo. Pubmedclip: How much does clip benefit visual question answering in the medical domain? In *Findings of the Association for Computational Linguistics: EACL 2023*, pages 1181–1193, 2023. [6](#)
- [9] Shansan Gong, Mukai Li, Jiangtao Feng, Zhiyong Wu, and LingPeng Kong. Diffuseq: Sequence to sequence text generation with diffusion models. *arXiv preprint arXiv:2210.08933*, 2022. [2](#)
- [10] Shansan Gong, Shivam Agarwal, Yizhe Zhang, Jiacheng Ye, Lin Zheng, Mukai Li, Chenxin An, Peilin Zhao, Wei Bi, Jiawei Han, et al. Scaling diffusion language models via adaptation from autoregressive models. *arXiv preprint arXiv:2410.17891*, 2024. [2](#)
- [11] Aaron Grattafiori, Abhimanyu Dubey, Abhinav Jauhri, Abhinav Pandey, Abhishek Kadian, Ahmad Al-Dahle, Aiesha Letman, Akhil Mathur, Alan Schelten, Alex Vaughan, et al. The llama 3 herd of models. *arXiv preprint arXiv:2407.21783*, 2024. [2](#)
- [12] Danfeng Guo and Demetri Terzopoulos. Prompting medical large vision-language models to diagnose pathologies by visual question answering. *arXiv preprint arXiv:2407.21368*, 2024. [2](#)
- [13] Daya Guo, Dejian Yang, Haowei Zhang, Junxiao Song, Ruoyu Zhang, Runxin Xu, Qihao Zhu, Shirong Ma, Peiyi Wang, Xiao Bi, et al. Deepseek-r1: Incentivizing reasoning capability in llms via reinforcement learning. *arXiv preprint arXiv:2501.12948*, 2025. [5](#)
- [14] Xuehai He, Yichen Zhang, Luntian Mou, Eric Xing, and Pengtao Xie. Pathvqa: 30000+ questions for medical visual question answering. *arXiv preprint arXiv:2003.10286*, 2020. [4](#), [13](#), [14](#)
- [15] Jonathan Ho, Ajay Jain, and Pieter Abbeel. Denoising diffusion probabilistic models. *Advances in neural information processing systems*, 33:6840–6851, 2020. [1](#)
- [16] Ting-Yao Hsu, Chieh-Yang Huang, Ryan Rossi, Sungchul Kim, C Lee Giles, and Ting-Hao K Huang. Gpt-4 as an effective zero-shot evaluator for scientific figure captions. *arXiv preprint arXiv:2310.15405*, 2023. [5](#)
- [17] Yuxiang Lai, Jike Zhong, Ming Li, Shitian Zhao, and Xiaofeng Yang. Med-r1: Reinforcement learning for generalizable medical reasoning in vision-language models. *arXiv preprint arXiv:2503.13939*, 2025. [2](#)
- [18] Jason J Lau, Soumya Gayen, Asma Ben Abacha, and Dina Demner-Fushman. A dataset of clinically generated visual questions and answers about radiology images. *Scientific data*, 5(1):1–10, 2018. [4](#), [13](#), [14](#)
- [19] Chunyuan Li, Cliff Wong, Sheng Zhang, Naoto Usuyama, Haotian Liu, Jianwei Yang, Tristan Naumann, Hoifung Poon, and Jianfeng Gao. Llava-med: Training a large language-and-vision assistant for biomedicine in one day. *Advances in Neural Information Processing Systems*, 36:28541–28564, 2023. [2](#), [3](#), [4](#), [5](#), [6](#), [12](#), [13](#), [14](#), [15](#), [16](#)
- [20] Pengfei Li, Gang Liu, Lin Tan, Jinying Liao, and Shenjun Zhong. Self-supervised vision-language pre-training for medical visual question answering. In *2023 IEEE 20th International Symposium on Biomedical Imaging (ISBI)*, pages 1–5. IEEE, 2023. [6](#)
- [21] Xiang Li, John Thickstun, Ishaan Gulrajani, Percy S Liang, and Tatsunori B Hashimoto. Diffusion-lm improves controllable text generation. *Advances in neural information processing systems*, 35:4328–4343, 2022. [2](#)
- [22] Weixiong Lin, Ziheng Zhao, Xiaoman Zhang, Chaoyi Wu, Ya Zhang, Yanfeng Wang, and Weidi Xie. Pmc-clip: Contrastive language-image pre-training using biomedical documents. In *International Conference on Medical Image Computing and Computer-Assisted Intervention*, pages 525–536. Springer, 2023. [1](#)
- [23] Bo Liu, Li-Ming Zhan, Li Xu, Lin Ma, Yan Yang, and Xiao-Ming Wu. Slake: A semantically-labeled knowledge-enhanced dataset for medical visual question answering. In *2021 IEEE 18th international symposium on biomedical imaging (ISBI)*, pages 1650–1654. IEEE, 2021. [4](#), [13](#), [14](#)
- [24] Haotian Liu, Chunyuan Li, Qingyang Wu, and Yong Jae Lee. Visual instruction tuning. *Advances in neural information processing systems*, 36:34892–34916, 2023. [3](#), [5](#), [13](#)
- [25] Haotian Liu, Chunyuan Li, Yuheng Li, and Yong Jae Lee. Improved baselines with visual instruction tuning. In *Proceedings of the IEEE/CVF conference on computer vision and pattern recognition*, pages 26296–26306, 2024. [3](#)
- [26] Yang Liu, Dan Iter, Yichong Xu, Shuohang Wang, Ruochen Xu, and Chenguang Zhu. G-eval: Nlg evaluation using gpt-4 with better human alignment. *arXiv preprint arXiv:2303.16634*, 2023. [5](#)

- [27] Yunyi Liu, Zhanyu Wang, Dong Xu, and Luping Zhou. Q2atransformer: Improving medical vqa via an answer querying decoder. In *International conference on information processing in medical imaging*, pages 445–456. Springer, 2023. 6
- [28] Aaron Lou, Chenlin Meng, and Stefano Ermon. Discrete diffusion modeling by estimating the ratios of the data distribution. *arXiv preprint arXiv:2310.16834*, 2023. 1, 3
- [29] Yizhen Luo, Jiahuan Zhang, Siqi Fan, Kai Yang, Yushuai Wu, Mu Qiao, and Zaiqing Nie. Biomedgpt: Open multimodal generative pre-trained transformer for biomedicine. *arXiv preprint arXiv:2308.09442*, 2023. 2
- [30] Rabeeh Karimi Mahabadi, Hamish Ivison, Jaesung Tae, James Henderson, Iz Beltagy, Matthew E Peters, and Arman Cohan. Tess: Text-to-text self-conditioned simplex diffusion. *arXiv preprint arXiv:2305.08379*, 2023. 2
- [31] Meta AI. Llama-3.2-11B-Vision: A Multimodal Vision–Language LLM. Model card via Meta AI, September 2024. Version released September 25, 2024; instruction-tuned for image reasoning, captioning, and VQA with 10.6B parameters. 5, 13
- [32] Michael Moor, Qian Huang, Shirley Wu, Michihiro Yasunaga, Yash Dalmia, Jure Leskovec, Cyril Zakka, Eduardo Pontes Reis, and Pranav Rajpurkar. Medflamingo: a multimodal medical few-shot learner. In *Machine Learning for Health (ML4H)*, pages 353–367. PMLR, 2023. 2, 5, 13
- [33] Shen Nie, Fengqi Zhu, Zebin You, Xiaolu Zhang, Jingyang Ou, Jun Hu, Jun Zhou, Yankai Lin, Ji-Rong Wen, and Chongxuan Li. Large language diffusion models. *arXiv preprint arXiv:2502.09992*, 2025. 1, 2, 3, 4, 7, 12, 13
- [34] OpenAI. Introducing gpt-4.1 in the api. <https://openai.com/index/gpt-4-1/>, April 2025. Includes GPT-4.1, GPT-4.1 mini, and GPT-4.1 nano. 5, 12
- [35] OpenAI, Josh Achiam, Steven Adler, Sandhini Agarwal, Lama Ahmad, Ilge Akkaya, . . . , and Barret Zoph. Gpt-4 technical report. <https://arxiv.org/abs/2303.08774>, 2023. arXiv:2303.08774, submitted March 15 2023. 5
- [36] Jingyang Ou, Shen Nie, Kaiwen Xue, Fengqi Zhu, Jiacheng Sun, Zhenguo Li, and Chongxuan Li. Your absorbing discrete diffusion secretly models the conditional distributions of clean data. *arXiv preprint arXiv:2406.03736*, 2024. 2, 3
- [37] Long Ouyang, Jeffrey Wu, Xu Jiang, Diogo Almeida, Carroll Wainwright, Pamela Mishkin, Chong Zhang, Sandhini Agarwal, Katarina Slama, Alex Ray, et al. Training language models to follow instructions with human feedback. *Advances in neural information processing systems*, 35:27730–27744, 2022. 5
- [38] Jiazen Pan, Che Liu, Junde Wu, Fenglin Liu, Jiayuan Zhu, Hongwei Bran Li, Chen Chen, Cheng Ouyang, and Daniel Rueckert. Medvilm-r1: Incentivizing medical reasoning capability of vision-language models (vlms) via reinforcement learning. *arXiv preprint arXiv:2502.19634*, 2025. 2, 5, 13
- [39] Alec Radford, Jong Wook Kim, Chris Hallacy, Aditya Ramesh, Gabriel Goh, Sandhini Agarwal, Girish Sastry, Amanda Askell, Pamela Mishkin, Jack Clark, et al. Learning transferable visual models from natural language supervision. In *International conference on machine learning*, pages 8748–8763. PMLR, 2021. 3
- [40] Samyam Rajbhandari, Olatunji Ruwase, Jeff Rasley, Shaden Smith, and Yuxiong He. Zero-infinity: Breaking the gpu memory wall for extreme scale deep learning. In *Proceedings of the international conference for high performance computing, networking, storage and analysis*, pages 1–14, 2021. 13
- [41] Pierre H Richemond, Sander Dieleman, and Arnaud Doucet. Categorical sdes with simplex diffusion. *arXiv preprint arXiv:2210.14784*, 2022. 2
- [42] Subham Sahoo, Marianne Arriola, Yair Schiff, Aaron Gokaslan, Edgar Marroquin, Justin Chiu, Alexander Rush, and Volodymyr Kuleshov. Simple and effective masked diffusion language models. *Advances in Neural Information Processing Systems*, 37:130136–130184, 2024. 1
- [43] Jiaxin Shi, Kehang Han, Zhe Wang, Arnaud Doucet, and Michalis Titsias. Simplified and generalized masked diffusion for discrete data. *Advances in neural information processing systems*, 37:103131–103167, 2024. 1
- [44] Jiaming Song, Chenlin Meng, and Stefano Ermon. Denoising diffusion implicit models. *arXiv preprint arXiv:2010.02502*, 2020. 1
- [45] Yang Song, Jascha Sohl-Dickstein, Diederik P Kingma, Abhishek Kumar, Stefano Ermon, and Ben Poole. Score-based generative modeling through stochastic differential equations. *arXiv preprint arXiv:2011.13456*, 2020. 1
- [46] Robin Strudel, Corentin Tallec, Florent Altché, Yilun Du, Yaroslav Ganin, Arthur Mensch, Will Grathwohl, Nikolay Savinov, Sander Dieleman, Laurent Sifre, et al. Self-conditioned embedding diffusion for text generation. *arXiv preprint arXiv:2211.04236*, 2022. 2
- [47] Hugo Touvron, Thibaut Lavril, Gautier Izacard, Xavier Martinet, Marie-Anne Lachaux, Timothée Lacroix, Baptiste Rozière, Naman Goyal, Eric Hambro, Faisal Azhar, et al. Llama: Open and efficient foundation language models. *arXiv preprint arXiv:2302.13971*, 2023. 3

- [48] Michael Tschannen, Alexey Gritsenko, Xiao Wang, Muhammad Ferjad Naeem, Ibrahim Alabdulmohsin, Nikhil Parthasarathy, Talfan Evans, Lucas Beyer, Ye Xia, Basil Mustafa, et al. Siglip 2: Multilingual vision-language encoders with improved semantic understanding, localization, and dense features. *arXiv preprint arXiv:2502.14786*, 2025. 4, 12, 13
- [49] Tom Van Sonsbeek, Mohammad Mahdi Derakhshani, Ivona Najdenkoska, Cees GM Snoek, and Marcel Worring. Open-ended medical visual question answering through prefix tuning of language models. In *International Conference on Medical Image Computing and Computer-Assisted Intervention*, pages 726–736. Springer, 2023. 6
- [50] Pascal Vincent. A connection between score matching and denoising autoencoders. *Neural computation*, 23(7):1661–1674, 2011. 3
- [51] Sheng Wang, Zihao Zhao, Xi Ouyang, Tianming Liu, Qian Wang, and Dinggang Shen. Interactive computer-aided diagnosis on medical image using large language models. *Communications Engineering*, 3(1):133, 2024. 2
- [52] Sicheng Wang, Che Liu, and Rossella Arcucci. How does diverse interpretability of textual prompts impact medical vision-language zero-shot tasks? *arXiv preprint arXiv:2409.00543*, 2024. 2
- [53] Zifeng Wang, Zhenbang Wu, Dinesh Agarwal, and Jimeng Sun. Medclip: Contrastive learning from unpaired medical images and text. In *Proceedings of the Conference on Empirical Methods in Natural Language Processing. Conference on Empirical Methods in Natural Language Processing*, volume 2022, page 3876, 2022. 1
- [54] Shanglong Yang, Zhipeng Yuan, Shunbao Li, Ruoling Peng, Kang Liu, and Po Yang. Gpt-4 as evaluator: Evaluating large language models on pest management in agriculture. *arXiv preprint arXiv:2403.11858*, 2024. 5
- [55] Jiasheng Ye, Zaixiang Zheng, Yu Bao, Lihua Qian, and Mingxuan Wang. Dinoiser: Diffused conditional sequence learning by manipulating noises. *arXiv preprint arXiv:2302.10025*, 2023. 2
- [56] Zebin You, Shen Nie, Xiaolu Zhang, Jun Hu, Jun Zhou, Zhiwu Lu, Ji-Rong Wen, and Chongxuan Li. Llada-v: Large language diffusion models with visual instruction tuning. *arXiv preprint arXiv:2505.16933*, 2025. 2, 4, 5, 12, 13
- [57] Kai Zhang, Jun Yu, Eashan Adhikarla, Rong Zhou, Zhiling Yan, Yixin Liu, Zhengliang Liu, Lifang He, Brian Davison, Xiang Li, et al. Biomedgpt: A unified and generalist biomedical generative pre-trained transformer for vision, language, and multimodal tasks. *arXiv e-prints*, pages arXiv–2305, 2023. 2
- [58] Sheng Zhang, Yanbo Xu, Naoto Usuyama, Jaspreet Bagga, Robert Tinn, Sam Preston, Rajesh Rao, Mu Wei, Naveen Valluri, Cliff Wong, et al. Large-scale domain-specific pretraining for biomedical vision-language processing. *arXiv preprint arXiv:2303.00915*, 2(3):6, 2023. 6
- [59] Wenhui Zhu, Xuanzhao Dong, Xin Li, Peijie Qiu, Xiwen Chen, Abolfazl Razi, Aris Sotiras, Yi Su, and Yalin Wang. Toward effective reinforcement learning fine-tuning for medical vqa in vision-language models. *arXiv e-prints*, pages arXiv–2505, 2025. 5, 13
- [60] Wenhui Zhu, Xin Li, Xiwen Chen, Peijie Qiu, Vamsi Krishna Vasa, Xuanzhao Dong, Yanxi Chen, Natasha Lepore, Oana Dumitrascu, Yi Su, et al. Retinalgpt: A retinal clinical preference conversational assistant powered by large vision-language models. *arXiv e-prints*, pages arXiv–2503, 2025. 5, 13

A. Implementation Details

A.1. Training Configuration

The training process of LLaDA-MedV is structured into three stages. Following the approach of [19], the first two stages aim to establish semantic alignment between biomedical language and visual content, while also enabling the model to follow visual instructions within a biomedical context. To further improve performance in dataset-specific scenarios, we introduce a third stage involving supervised fine-tuning (SFT) on three biomedical VQA datasets.

Throughout all stages, we employ LLaDA-8B-Instruct [33] as the language backbone. The vision tower is based on SigLIP2 [48], and the vision-language projection module is implemented as a lightweight two-layer MLP with GELU activation. All training is conducted using four NVIDIA A100 GPUs (80GB each). Additional training details are provided in Tab. 6.

A.2. Inference Procedure

Inference Details. The response generation process simulates the reverse dynamics of mask diffusion. Starting from a fully masked response (i.e., $t = 1$), the learned mask predictor p_θ iteratively reconstructs the assistant’s response. To better align with the reverse diffusion process, an appropriate remasking strategy is applied at each step. The detailed inference procedure is presented in Algorithm 1.

Algorithm 1 Inference Strategy in LLaDA-MedV

Require: Trained mask predictor p_θ , user visual input X_v , text prompt u_0 , response length L , and total sampling steps Z

Ensure: Start with fully masked response r_1 of length L (i.e., $t = 1$)

- 1: **for** t from 1 down to $1/Z$ with step $1/Z$ **do**
- 2: Set $s = t - 1/Z$
- 3: Predict $r_0 = \arg \max p_\theta(r_0 \mid X_v, u_0, r_t)$
- 4: **for** $i = 1$ to L **do**
- 5: **if** $r_t^i \neq M$ **then**
- 6: Set $r_0^i = r_t^i$ {Retain meaningful token}
- 7: **else**
- 8: Remask $r_0^i = M$ with probability s/t
- 9: **end if**
- 10: **end for**
- 11: **end for**
- 12: **return** r_0

Following prior works [33, 56], we adopt the low-confidence remasking strategy [5], in which only tokens with low confidence (i.e., lower p_θ values) are remasked at each step (e.g., Step 8), rather than selecting tokens uniformly at random. In addition, we explore a semi-autoregressive generation strategy [33]. Specifically, when

$B < L$, the response of length L is divided into L/B blocks, where B denotes the block length. Generation proceeds sequentially from left to right across blocks, with each block undergoing $Z \cdot B/L$ sampling steps (i.e., as noted in Algorithm 1).

For the main open-ended biomedical conversation tasks, we apply this strategy with $L = 256$, $B = 64$, and $Z = 256$. However, for downstream biomedical VQA tasks, we disable the semi-autoregressive mechanism by setting $L = B = Z = 64$. Unless otherwise specified, this setting is used consistently in all detailed analyses.

Baseline Model Configuration. We compare LLaDA-MedV against nine baseline vision-language models, covering both general-domain and biomedical-specific systems. These models are evaluated using their default system prompts and a maximum token limit of 256. For fairness, models with intermediate reasoning capabilities (e.g., MedVLM-R1) are evaluated using the full generated response.

In the open-ended biomedical conversation setting, we use GPT-4.1 mini [34] to assess performance, as the original GPT-4 (0314) used in [19] is no longer publicly accessible. Additionally, Tab. 7 provides an overview of all baseline models included in this evaluation. For downstream VQA benchmarks, we report baseline results directly from [19] when available, and therefore omit redundant model-specific details for clarity. We kindly refer readers to [19] for comprehensive baseline configurations in the VQA setting.

A.3. Dataset

Training dataset. We adopt the training data introduced in [19] to equip LLaDA-MedV with biomedical visual understanding capabilities across three training stages. All images are processed using the SigLIP2 vision encoder [48].

- **Stage 1.** We use 600K aligned image-text pairs to train the vision-language projection module and learn robust cross-modal representations. Each training instance is structured as a single-turn dialogue, where the human prompt is removed except for a special `<image>` token. This setup ensures that the model learns to generate responses conditioned solely on image embeddings, without reliance on textual input.
- **Stage 2.** We leverage a 60K multi-turn dialogue dataset with inline entity mentions. Each instance contains a full conversation between a human and the assistant, where image embeddings are prepended only to the first human input. This configuration enables the model to follow visually grounded instructions across multiple dialogue turns.
- **Stage 3.** We perform supervised fine-tuning using the training sets from three biomedical VQA datasets: VQA-

Training stage	Alignment	MD-SFT	SD-SFT (VQA-RAD)	SD-SFT(SLAKE)	SD-SFT(PathVQA)
Vision tower			Siglip2-so400m-patch14-384 [48]		
Language tower			LLaDA-8B-Instruct [33]		
Projector			2-layer MLP with GELU		
Attention			Bidirectional attention		
DeepSpeed			ZeRO-3 [40]		
Optimizer			AdamW		
Scheduler			Cosine scheduler with 3% warmup		
Batch size (Global)	32	8	8	8	8
Model max length	8192	8192	8192	8192	8192
#Samples in training set	600K	60k	1797	4919	19755
LR of language tower	-	1×10^{-5}	2×10^{-6}	2×10^{-6}	2×10^{-6}
LR of projector	1×10^{-3}	1×10^{-5}	2×10^{-6}	2×10^{-6}	2×10^{-6}
Epoch	2	4	2	10	7

Table 6. Training configurations of LLaDA-MedV across three stages. **MD-SFT** denotes the multi-turn dialogue SFT, and **SD-SFT** represent the single-turn dialogue over training set of VQA-RAD, SLAKE and PathVQA, respectively.

Table 7. Overview of baseline models evaluated on the open-ended biomedical conversation task. The **Domain** column indicates whether each model is general-purpose or biomedical-specific. The **Size** column refers to the model size, where specified. Detailed model variants are included when available.

Model	Domain	Size	Variant / Backbone
LLaMA [31]	General	11B	LLaMA-3.2-11B-Vision
LLaVA [24]	General	7B	llava-1.5-7B
LLaVA-Med [19]	Biomedical	7B	llava-med-v1.5-mistral-7B
Med-Flamingo [32]	Biomedical	9B	Med-Flamingo-9B
MedVLM-R1 [38]	Biomedical	-	-
Qwen-RL-Med [59]	Biomedical	-	-
Qwen-VL [2]	General	2B	Qwen2-VL-2B-Instruct
RetinalGPT [60]	Biomedical	-	-
LLaDA-V [56]	General	-	-

RAD [18], SLAKE [23], and PathVQA [14]. Each VQA sample is converted into a one-turn dialogue, where the question is treated as the human input and the ground-truth answer is used as the assistant’s response. This training simulates the multi-turn dialogue structure introduced in Stage 2.

Open-end Biomedical Conversation Benchmark. We use the open-ended biomedical conversation benchmark proposed in [19] to evaluate model performance in realistic scenarios. Specifically, the dataset contains 193 novel questions paired with 50 corresponding images. Notably, these 50 image-caption pairs are entirely unseen during training.

The questions fall into two categories: open-ended conversations and detailed descriptions. Conversation-style questions are typically broad biomedical queries related to the image content, while detailed description questions explicitly ask for fine-grained analysis of the visual information. As previously mentioned, ground-truth responses are generated by GPT-4 (i.e., GPT-4-0314) based solely on the associated figure captions. To evaluate the candidate model’s response (e.g., from LLaDA-MedV), we use GPT-4.1 mini as the automatic evaluator. GPT-4.1 mini is provided with both the candidate response and the GPT-4 reference response, along with the original question, image caption, and relevant context. It is then prompted to rate each response

across four dimensions, including helpfulness, relevance, accuracy, and level of detail, and to assign an overall score on a scale from 1 to 10, where higher scores indicate better performance. Additionally, GPT-4.1 mini provides a detailed rationale for each evaluation, facilitating more transparent comparisons. The final score for the candidate model is normalized by the GPT-4 reference score to compute a relative performance metric.

Downstream Biomedical Visual Question Answering.

Following [19], we use three biomedical visual question answering (VQA) benchmarks to further improve LLaDA-MedV performance in scenario that require high service quality. We outlined the detailed statistics in Tab. 8.

- **VQA-RAD** [18] consists of 3,515 clinician-generated QA pairs grounded in 315 radiology images, which are evenly distributed across three anatomical regions: head, chest, and abdomen. Each image is paired with multiple questions, covering a diverse range of clinical inquiries. The questions are categorized into 11 distinct types, including abnormality, attribute, modality, organ system, color, counting, object or condition presence, size, imaging plane, positional reasoning, and others. Approximately half of the answers are closed-ended (i.e., yes/no), while the remaining are open-ended, typically expressed as a single word or short phrase. It is worth noting that we use the cleaned version of the dataset in all experiments, resulting in a total of 2,248 QA pairs.
- **SLAKE** [23] is a Semantically-Labeled Knowledge-Enhanced benchmark designed for medical visual question answering. It contains 642 radiology images and over 7,000 diverse question-answer pairs, all annotated by experienced physicians. Many of the questions require external medical knowledge, which is supported by an accompanying medical knowledge graph. The dataset also provides rich visual annotations, including semantic segmentation masks and object detection bounding boxes. In addition, SLAKE encompasses a broader range of imaging modalities and anatomical regions compared to existing datasets, covering areas such as the brain, neck, chest, abdomen, and pelvic cavity. Here, we only consider the English subset throughout the experiments.
- **PathVQA** [14] is a VQA benchmark consisting of pathology images. It includes 4,998 images accompanied by 32,799 question-answer pairs. Each image is associated with multiple questions addressing various aspects such as location, shape, color, and appearance. The questions are categorized into two main types: open-form (e.g., “what,” “why,” “how,” “where”) and closed-form, encompassing a wide range of question styles relevant to pathology interpretation.

We evaluate the performance of LLaDA-MedV and report baseline results outlined in [19] across all three VQA bench-

marks, where available. However, for more detailed analysis, we focus exclusively on VQA-RAD and SLAKE to ensure evaluation efficiency.

Dataset Details	VQA-RAD		SLAKE			PathVQA		
	Train	Test	Train	Val	Test	Train	Val	Test
# Images	313	203	450	96	96	2599	858	858
# QA	1797	451	4919	1053	1061	19755	6279	6761
# Closed-form	1027	272	1943	422	416	9806	3135	3391
# Open-form	770	179	2976	631	645	9949	3144	3370

Table 8. Statistics of the downstream VQA benchmarks. # denotes the number of samples in each split.

B. Visualization Analysis

B.1. Open-end Biomedical Conversation

Due to space limitations in the main text, we provide additional visualizations for open-ended biomedical conversations in Fig. 5, Fig. 6, and Fig. 7. As shown, LLaDA-MedV consistently produces relatively longer responses enriched with more contextual information. For all visualized examples, we use the following generation settings (as used in main setting): $L = 256$, $B = 64$, and $Z = 256$. For clarity, we omit GPT-4 reference answer.

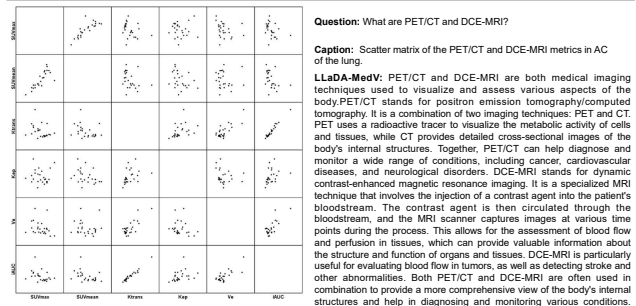


Figure 5. Illustration of LLaDA-MedV response in open-end biomedical conversation task. Image, question and corresponding caption comes from [19]

B.2. Biomedical VQA

We provide additional visualizations of LLaDA-MedV responses on downstream biomedical VQA tasks. For this experiment, we set $L = B = Z = 64$. Prior models often treat open-form questions as a classification problem over a fixed set of predefined answers (e.g., distinct answers seen during training) [19], which raises concerns about generalizability. In contrast, as illustrated in Fig. 8, LLaDA-MedV struggle with reliably selecting from predefined candidate sets due to limited post-training. Instead, it tends to generate more open-ended responses, which are less constrained and

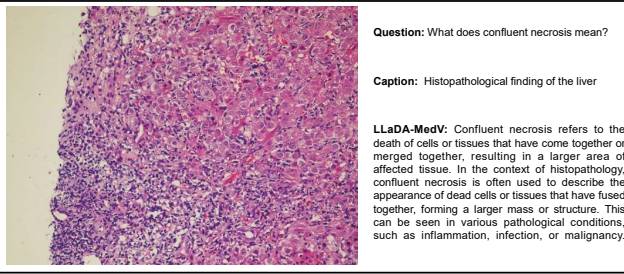


Figure 6. Illustration of LLaDA-MedV response in open-end biomedical conversation task. Image, question and corresponding caption comes from [19]

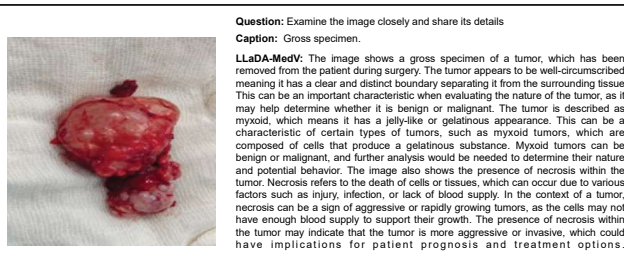


Figure 7. Illustration of LLaDA-MedV response in open-end biomedical conversation task. Image, question and corresponding caption comes from [19]

may deviate from rigid answer formats typically expected in evaluation.

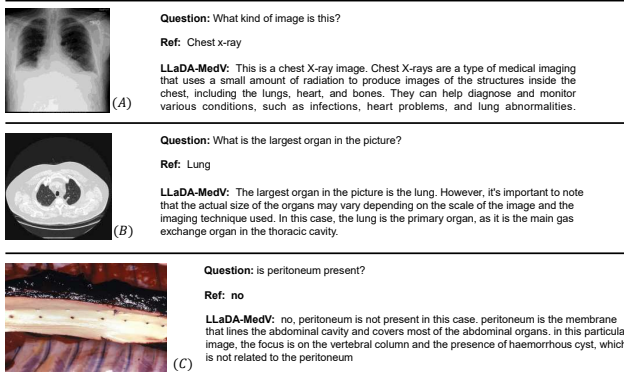


Figure 8. Illustration of LLaDA-MedV responses on downstream VQA tasks across three benchmarks. (A) corresponds to a QA example from VQA-RAD, (B) from SLAKE, and (C) from PathVQA. **Ref** denotes the ground-truth answer.

B.3. Inference-Time Key Factors

In our investigation of inference-time factors influencing LLaDA-MedV, we systematically evaluate the effects of response length (L), block length (B), and the number of sampling steps (Z) on final generation quality. This section is

dedicated to providing additional visualizations to facilitate a deeper understanding of their impact.

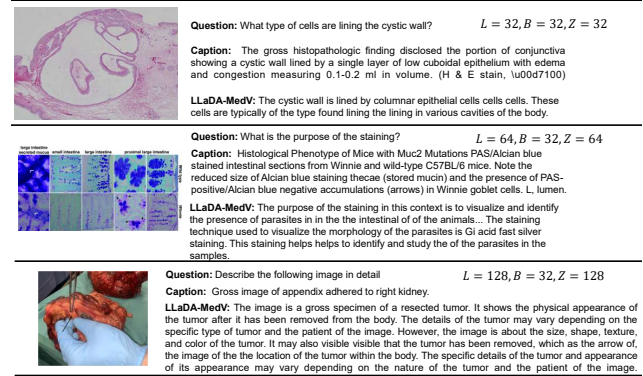


Figure 9. Illustration of LLaDA-MedV responses on open-end biomedical conversation as response length L changes. Image, question and corresponding caption comes from [19]. We omit GPT-4 reference answer for clarity.

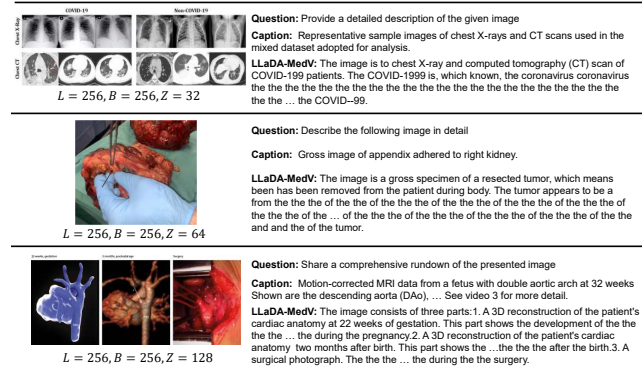


Figure 10. Illustration of LLaDA-MedV responses on open-end biomedical conversation as sampling steps Z changes. Image, question and corresponding caption comes from [19]. We omit GPT-4 reference answer for clarity.

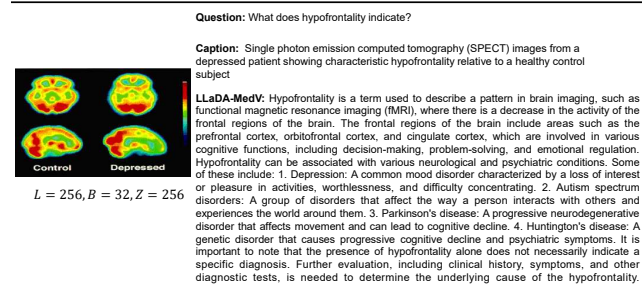


Figure 11. Illustration of LLaDA-MedV responses on open-end biomedical conversation as block length B changes. Image, question and corresponding caption comes from [19]. We omit GPT-4 reference answer for clarity.



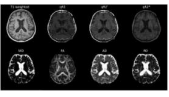
Question: Are there any signs of lymph node involvement?

Caption: Chest X-ray: Normal with no signs of metastatic lesions

LLaDA-MedV: The chest X-ray does not show any signs of lymph node involvement. However, it is important to remember that a chest X-ray is just one diagnostic tool, and further evaluation, such as a CT scan or MRI, may be necessary to rule out any potential lymph node involvement or other underlying conditions.

$L = 256, B = 128, Z = 256$

Question: Describe the following image in detail



Caption: Selected slice from a multi-modal MRI dataset of a patient with Parkinson's disease

LLaDA-MedV: The image is an MRI (Magnetic Resonance Imaging) scan of the brain. It includes three types of sequences: 1. T1-weighted, 2. T2-weighted, and diffusion-weighted imaging (DWI). 1. T1-weighted images: These are the most common type of MRI sequence and provide good contrast between different tissues. They typically show bright areas of water (nerves) and dark areas of fat (muscle). 2. T2-weighted images: These images are similar to T1-weighted images but provide different contrast between different tissues. They typically show dark areas of water (nerves) and bright areas of fat (muscle). 3. Diffusion-weighted imaging (DWI): DWI is a specialized MRI technique that measures the diffusion of water molecules within tissues. It is particularly useful for detecting changes in tissue microstructure, such as those caused by inflammation, tumors, or other pathological processes. In this particular image, the T1-weighted, T2-weighted, and DWI sequences are used to visualize different aspects of the brain, such as the distribution of water, the presence of fat, and the movement of water molecules within the tissue. This can help healthcare professionals diagnose and monitor various neurological conditions and assess the effectiveness of treatments.

Figure 12. Illustration of LLaDA-MedV responses on open-end biomedical conversation as block length B changes. Image, question and corresponding caption comes from [19]. We omit GPT-4 reference answer for clarity.

Specifically, We observe that variations in the generation length L impact overall performance in open-ended biomedical conversation tasks, as shown in Fig. 9. This discrepancy may raise initial concerns about the fairness of our comparisons, since longer responses typically provide richer context to GPT-based evaluators, potentially leading to higher perceived answer quality. However, we emphasize that all evaluations are conducted under a controlled setting in which models are encouraged to generate responses of fixed length ($L = 256$). For ARMs such as LLaVA-Med, this constraint is enforced by setting the maximum token length to 256. In contrast, LLaDA-MedV leverages a masked prediction mechanism, which inherently encourages the generation of more complete and informative responses within the same length constraint. Additionally, differences in benchmark design and evaluation protocols may also contribute to the observed variation in performance trends. We further find that the number of sampling steps Z plays an important role in controlling response diversity. As shown in Fig. 10, when generating long responses, an insufficient number of steps can lead to noticeable token repetition. Lastly, when using semi-autoregressive generation, the choice of block length B must be made with care. To aid understanding, we provide qualitative visualizations in Fig. 11 and Fig. 12.